



$W\gamma$ production at DØ with $L = 4.2 \text{ fb}^{-1}$ data

The DØ Collaboration
URL <http://www-d0.fnal.gov>
(Dated: March 11, 2011)

We describe a search for $WW\gamma$ anomalous couplings and cross section measurement for $W\gamma$ production using 4.2 fb^{-1} Run IIb DØ data in the muon channel. We set limits on anomalous $WW\gamma$ couplings at the 95% C.L. The one dimensional 95% C.L. limits are $-0.14 < \Delta\kappa_\gamma < 0.15$ and $-0.02 < \lambda_\gamma < 0.02$. The cross section times branching fraction for the process $p\bar{p} \rightarrow W\gamma + X \rightarrow \mu\nu\gamma + X$ with $p_T^\gamma > 8 \text{ GeV}$ and $\Delta R_{\mu\gamma} > 0.7$ is measured to be $15.2 \pm 0.4 \text{ (stat)} \pm 1.6 \text{ (syst) pb}$, which agrees with the SM expectation of $16.0 \pm 0.4 \text{ pb}$.

I. INTRODUCTION

The electroweak theory of the Standard Model (SM) has been remarkably successful in describing the all experiments to date. The $WW\gamma$ vertex is an example of self-interactions of electroweak bosons. Such interactions are a consequence of $SU(2)_L \times U(1)_Y$ gauge symmetry of the SM. In this analysis, we use the production of $p\bar{p} \rightarrow W\gamma \rightarrow \mu\nu\gamma$ events to study this vertex and set limits on non-SM $WW\gamma$ couplings.

An effective Lagrangian parameterizes the $WW\gamma$ coupling and, for CP-conserving couplings, has two coupling parameters κ_γ and λ_γ . They are related to the magnetic and electric dipoles of the W boson, respectively. For the SM, $\kappa = 1$ and $\lambda = 0$, leading to a more convenient notation of $\Delta\kappa = \kappa - 1 = 0$. If there is new physics leading to different, or anomalous, coupling values, then the $W\gamma$ cross section will increase and the photon is more energetic than in the SM case.

In $p\bar{p}$ collisions, the three Born level Feynman diagrams for $W\gamma$ with leptonic decay are shown in Fig. 2. Interference between these three amplitudes produces a zero amplitude at a specific angle θ^* between the W and incoming quark (see Fig. 1a). At hadron colliders the longitudinal momentum of the neutrino from W decays is unknown, and so the angular distribution θ^* used to probe the radiation amplitude zero is difficult to measure directly. However, as shown in Ref. [3], the radiation amplitude zero is also visible in the charge-signed photon-lepton rapidity difference as a dip around -0.3 as shown in Fig. 1b. Thus, we measure the charge-signed photon-lepton rapidity difference from our experiments to study the radiation amplitude zero. A major challenge for this study is the final state radiation (FSR) contribution (see Fig. 3), which obscures the SM radiation amplitude zero.

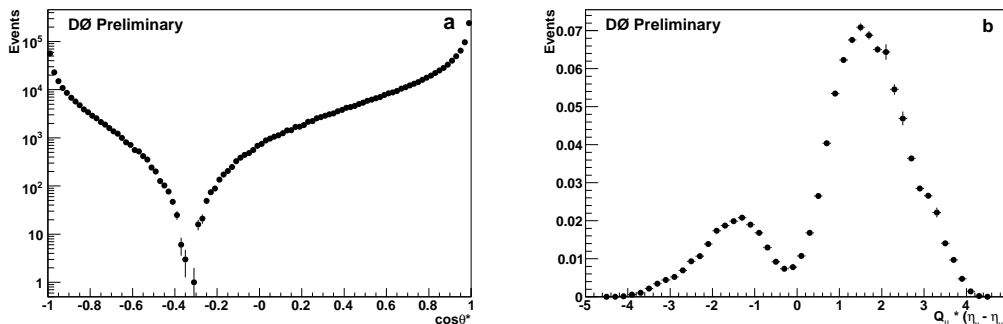


FIG. 1: Left plot shows $\cos\theta^*$ between the W and incoming quark in $W\gamma$ rest frame from PYTHIA [1]. Right plot shows the charge-signed photon-lepton rapidity difference from next-to-leading order $W\gamma$ generator [2, 3]

In PYTHIA $W\gamma$ production does not include the FSR process. To compensate for that, in this analysis, the $W\gamma$ signal events are generated from leading-order $W\gamma$ generator [2], and processed through PYTHIA to include parton showering and hadronization. Further the photon E_T spectrum is reweighted to the NLO [3] calculation to take into account the higher order correction.

II. DØ DETECTOR AND DATA SAMPLE

The DØ detector is comprised of a central tracking system in a 2 T super-conducting solenoidal magnet, a liquid-argon/uranium calorimeter, a central preshower detector and a muon spectrometer [4]. The major parts of the DØ detector used in event selection are the tracking system, the electromagnetic (EM) calorimeter, the central preshower detector (CPS) and muon system. The tracking system consists of a silicon microstrip tracker (SMT) and an eight-layer scintillating fiber tracker (CFT) mounted on thin coaxial barrels. It provides coverage for charged particles in the pseudo-rapidity range $|\eta| < 3$ (where the pseudo-rapidity is defined as $\eta \equiv -\ln[\tan(\frac{\theta}{2})]$, with θ denoting the polar angle with respect to the proton beam direction.) The calorimeter has a central section (CC) covering up to $|\eta| \approx 1.1$, and two end components (EC) extending coverage to $|\eta| \approx 4.2$. Each section is housed in a separate cryostat, and divided into EM layers on the inside and hadronic layers on the outside. The EM calorimeter has four longitudinal layers and transverse segmentation of 0.1×0.1 in $\eta - \phi$ space (where ϕ is the azimuthal angle), except in the third layer, where it is 0.05×0.05 . Immediately before the inner layer of the central EM calorimeter, there is a central preshower detector (CPS) formed of $2X_0$ of absorber followed by several layers of scintillating strips with embedded wavelength-shifting fibers. The muon system resides beyond the calorimeter and consists of a layer of tracking detectors and scintillation trigger counters before 1.8 T toroidal magnets, followed by two similar layers after

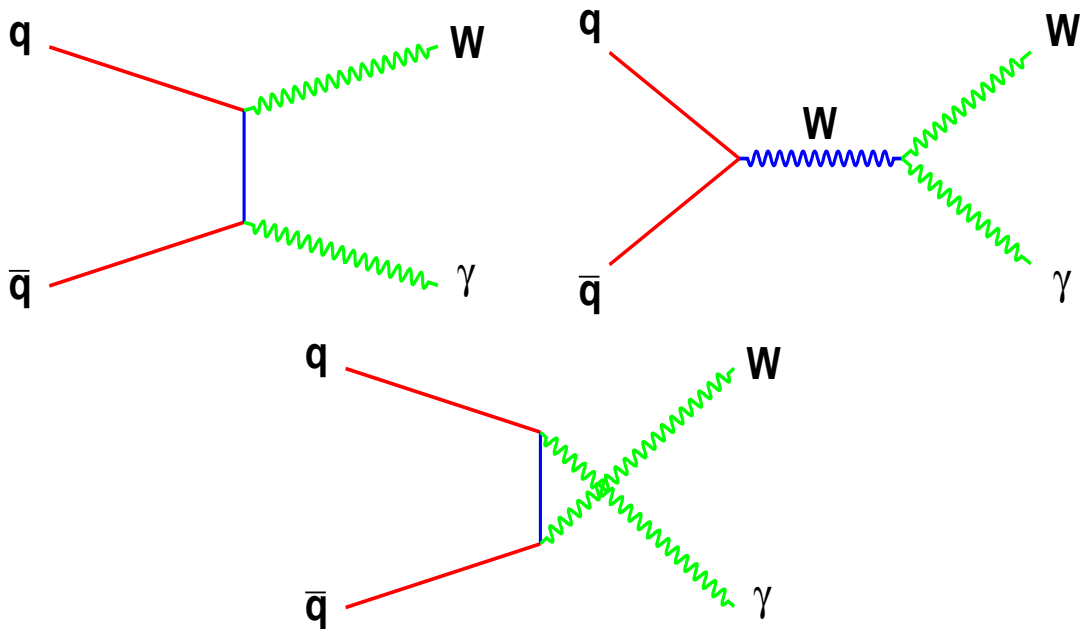


FIG. 2: Born level subprocesses for $W\gamma$ production in hadron collision: t channel process (top-left), s channel (top-right), u channel (bottom).

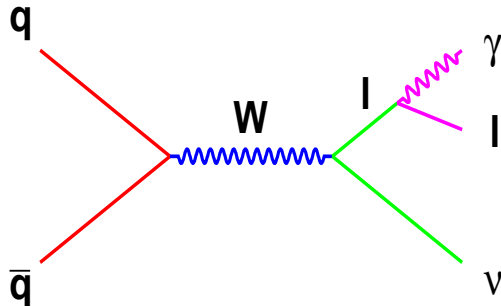


FIG. 3: Final state radiation from the charged lepton from W-decay.

the toroids. Luminosity is measured using plastic scintillator arrays located in front of the EC cryostats, covering $2.7 < |\eta| < 4.4$. The data acquisition system consists of a three-level trigger, designed to accommodate the high instantaneous luminosity. The data samples used in this analysis were collected between August 2007 and September 2009 and correspond to an integrated luminosity of 4.2 fb^{-1} .

III. EVENT SELECTION

Muons are selected with requirements: Muon candidates (as initiated by a track segment in the muon chambers) are selected with the following: (i) matching a $p_T > 20 \text{ GeV}$ and $|\eta| < 1.6$ central track, which should have at least 1 SMT hit; (ii) the sum of the transverse energy of calorimeter cells in the annulus $0.1 < \mathcal{R} = \sqrt{(\Delta\eta)^2 + (\Delta\phi)^2} < 0.4$ around the muon direction must be less than 2.5 GeV , and the sum of the transverse momentum of all tracks besides the muon track within $\mathcal{R} = 0.5$ must be less than 2.5 GeV .

Missing transverse energy \cancel{E}_T is required to be greater than 20 GeV , and $M_T > 40 \text{ GeV}$, where M_T is the transverse mass of the selected muon candidate and \cancel{E}_T .

Photons are selected from EM clusters reconstructed within a cone with radius $\mathcal{R} = 0.2$ in central ($-1.1 < \eta < 1.1$) or forward ($1.5 < |\eta| < 2.5$) calorimeter regions by requiring: (i) transverse energy E_T is greater than 10 GeV , (ii) at least 90% of the cluster energy is deposited in the EM calorimeter, (iv) the calorimeter isolation variable $I = [E_{\text{tot}}(0.4) - E_{\text{EM}}(0.2)]/E_{\text{EM}}(0.2)$ is less than 0.15, where $E_{\text{tot}}(0.4)$ is the total energy in a cone of radius $\mathcal{R} = 0.4$

and $E_{EM}(0.2)$ is the EM energy in a cone of radius $\mathcal{R} = 0.2$; (iv) the energy-weighted shower width squared in the $r - \phi$ plane in EM3 is consistent with the EM object, and (v) the scalar sum of the p_T of all tracks originating from the primary vertex in an annulus of $0.05 < \mathcal{R} < 0.4$ around the cluster ($p_{T\text{trk}}^{\text{sum}}$) is less than 2 (1.5) GeV in CC (EC). To suppress electrons misidentified as photons, the EM clusters are required to not be spatially matched to tracker activity, either a reconstructed track, or a set of hits in the SMT and CFT consistent with that of an electron. The contribution of jets misidentified as photons is reduced by combining the information from a set of variables sensitive to differences between photons and jets in the tracker activity and in the energy distributions in the calorimeter and CPS, using an artificial neural network discriminant O_{NN} [5]. For this analysis, $O_{NN} > 0.75$ is used.

To reduce the $Z_{\mu\mu}\gamma$ background, we veto the events if there exists an additional $p_T > 15$ GeV track except the muon associated one. To reduce the FSR contribution, we require the photon is away from the muon by $\mathcal{R} > 0.7$, and three-body (μ , \cancel{E}_T and γ) transverse mass $M_T^{\mu\gamma\cancel{E}_T}$ (see Eq. 1) greater than 110 GeV.

$$M_T^{\mu\gamma\cancel{E}_T} = \sqrt{(\sqrt{M_{\mu\gamma}^2 + |\mathbf{p}_T(\gamma) + \mathbf{p}_T(\mu)|^2} + \cancel{E}_T)^2 - |\mathbf{p}_T(\gamma) + \mathbf{p}_T(\mu) + \cancel{E}_T|^2} \quad (1)$$

IV. BACKGROUNDS

There are four major sources of background in this analysis: (i) events with $e\mu + X$ final state, where the electron is misidentified as photon due to tracking inefficiency; (ii) W +jet production, where the jet is misidentified as the photon; (iii) $Z_{\mu\mu}\gamma$ production, where one of the muon is lost; (iv) $W_{\tau\nu}\gamma$ production, where τ further decays to μ .

A. $e\mu + X$ background

The $e\mu + X$ background is composed of events where the electron is misidentified as a photon due to tracking inefficiencies, and mainly comes from the di-boson production. To estimate its contribution, we select an orthogonal data sample by requiring the EM cluster be matched with a good track. Then the ratio for EM cluster matching a good track and passing the photon no-track requirement is measured from the $Z \rightarrow ee$ data with parameterizing as a function of η . Finally, the $e\mu + X$ contribution is calculated with multiplying the ratio on the orthogonal sample.

B. W +jet background

The dominant background for this analysis is W +jet production. We use two different data driven methods to estimate the contribution. In method one, we select an orthogonal data sample by using the same selection criteria as described in section III, except reversing the photon $p_{T\text{trk}}^{\text{sum}}$ or shower width requirement. Thus, we select a W +bad photon data sample. Then we measure the ratio of jet passing the good photon selection criteria (see section III) and failing the $p_{T\text{trk}}^{\text{sum}}$ or shower width requirement from the multi-jet data. This ratio is measured as a function of E_T in 5 η regions for photon in CC and EC respectively. The final W +jet contribution is obtained with applying these ratios to the selected W +bad photon data events. In method two, we perform a fit on the photon O_{NN} distributions in 5 η regions for photon in CC and EC respectively. The photon O_{NN} templates are obtained from photon and jet Monte Carlo simulation, since the O_{NN} is well modelled [5, 6]. The results from these two methods are consistent, except the O_{NN} template fitting results suffers from the data statistics. We use the results from reversing photon quality cuts as the default.

C. $Z_{\mu\mu}\gamma$ and $W_{\tau\nu}\gamma$ backgrounds

Small backgrounds from $Z_{\mu\mu} + \gamma$, where one of the muons from Z decays is lost, and $W_{\tau\nu} + \gamma$, where the τ decays to a μ , are estimated from PYTHIA Drell-Yan $Z/\gamma^* \rightarrow \mu\mu$ and $W_{\tau\nu} + \gamma$ MC respectively.

V. SYSTEMATIC UNCERTAINTIES

In this analysis, we consider the following systematic uncertainties:

- 6.1% uncertainty on the total luminosity [7];
- 5% uncertainty on the single muon trigger efficiency;
- 3 – 10% uncertainty on the photon identification;
- 5% uncertainty on the muon identification;
- 0.9% uncertainty on the track veto;
- the influence of the parton distribution functions (PDF) uncertainty on the acceptance is 0.04%, estimated from CTEQ6M [8] error functions;
- $\sim 10\%$ uncertainty from the ratio of jet passing good photon criteria and reversed photon quality cuts.

VI. RESULTS

The number of data, background and predicted signal events are shown in Table I.

	γ in CC	γ in EC	Total
$e\mu+X$	0.2 ± 0.1	5.0 ± 1.9	5.2 ± 1.9
$Z_{\mu\mu}\gamma$	12.7 ± 1.7	8.6 ± 1.2	21.3 ± 2.6
$W_{\tau\nu}\gamma$	2.6 ± 0.4	3.6 ± 0.5	6.2 ± 0.8
W+jet	53.4 ± 5.7	48.1 ± 5.2	101.5 ± 7.7
total background	68.8 ± 6.0	65.4 ± 5.8	134.2 ± 8.6
data	233	259	492
data - background	164.2 ± 16.4	193.6 ± 17.1	357.8 ± 23.8
signal	171.6 ± 20.0	204.0 ± 23.4	375.6 ± 41.5

TABLE I: The number of data, background and predicted SM $W\gamma$ signal events.

Fig. 4 shows the final charge signed photon-muon rapidity difference from background subtracted data, SM and anomalous coupling ($\Delta\kappa_\gamma = -2, \lambda_\gamma = 0$) $W\gamma$ signal. The distribution in Fig. 4 shows a deficit near -0.3 that is consistent with the presence of the expected radiation amplitude zero.

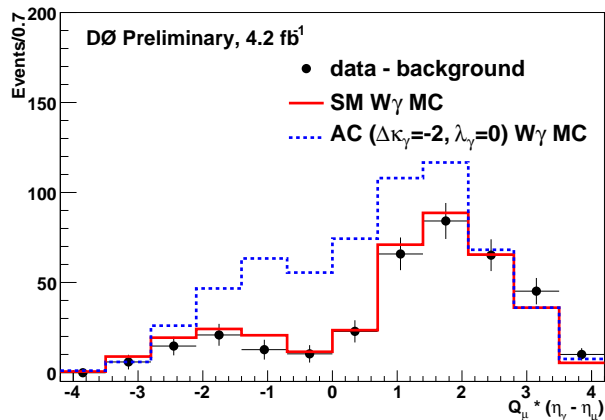


FIG. 4: Charge signed photon-muon rapidity difference for SM $W\gamma$ signal, anomalous coupling ($\Delta\kappa_\gamma = -2, \lambda_\gamma = 0$) $W\gamma$ signal and background subtracted data events.

The data is consistent with the SM prediction, we proceed to set the upper limits on the anomalous $WW\gamma$ coupling parameters $\Delta\kappa_\gamma$ and λ_γ . In the SM, $\Delta\kappa_\gamma = 0$ and $\lambda_\gamma = 0$. In the non-SM, the anomalous $WW\gamma$ couplings will give higher cross section than the SM prediction, especially the increase of the energetic photons. Due to the violation of unitarity at high energies for the anomalous couplings, a form factor with a scale Λ is introduced to modify the couplings parameters with $a_0 \rightarrow a_0/(1 + \hat{s}/\Lambda^2)^2$ where $a_0 = \Delta\kappa_\gamma, \lambda_\gamma$, and $\sqrt{\hat{s}}$ is the $W\gamma$ invariant mass. In this

analysis, $\Lambda = 2$ TeV is used and the photon transverse energy distributions (see Fig. 5) are used for the limits setting. The limits are calculated at the 95% confidence level (C.L.) using χ^2 fit. The one-dimensional 95% CL limits for the anomalous couplings are measured to be $-0.14 < \Delta\kappa_\gamma < 0.15$ and $-0.02 < \lambda_\gamma < 0.02$. Fig. 6 shows the corresponding results, with the contour showing the two-dimensional 95% C.L. exclusion limits, horizontal and vertical lines showing the one-dimensional 95% C.L. exclusion limits. By comparison with the latest Tevatron results [9] using both electron and muon channels (see Table II), the limits are improved by more than a factor of three, using a factor of six larger dataset. Except the luminosity increase, the major improvement is achieved by using novel and powerful photon O_{NN} to reduce the jet background. We also derive the 68% one-dimensional limits and compare the results with LEP experiments [10] in Table III. We have reached the similar sensitivity as the LEP experiments with this analysis.

DØ 0.7 fb^{-1} (combined e and μ channels)	$-0.51 < \Delta\kappa_\gamma < 0.51$	$-0.12 < \lambda_\gamma < 0.13$
DØ 4.2 fb^{-1} (μ channel)	$-0.14 < \Delta\kappa_\gamma < 0.15$	$-0.02 < \lambda_\gamma < 0.02$

TABLE II: 95% C.L. one-dimensional limits on the $\Delta\kappa_\gamma$ and λ_γ from recent Tevatron results [9] and the current analysis.

ALEPH	$-0.1 < \Delta\kappa_\gamma < 0.029$	$-0.043 < \lambda_\gamma < 0.014$
L3	$-0.049 < \Delta\kappa_\gamma < 0.095$	$-0.062 < \lambda_\gamma < 0.019$
OPAL	$-0.1 < \Delta\kappa_\gamma < 0.018$	$-0.097 < \lambda_\gamma < -0.024$
LEP2 combined	$-0.072 < \Delta\kappa_\gamma < 0.017$	$-0.049 < \lambda_\gamma < 0.008$
DØ 4.2 fb^{-1}	$-0.07 < \Delta\kappa_\gamma < 0.07$	$-0.012 < \lambda_\gamma < 0.011$

TABLE III: 68% C.L. one-dimensional limits on the $\Delta\kappa_\gamma$ and λ_γ from LEP and the current analysis.

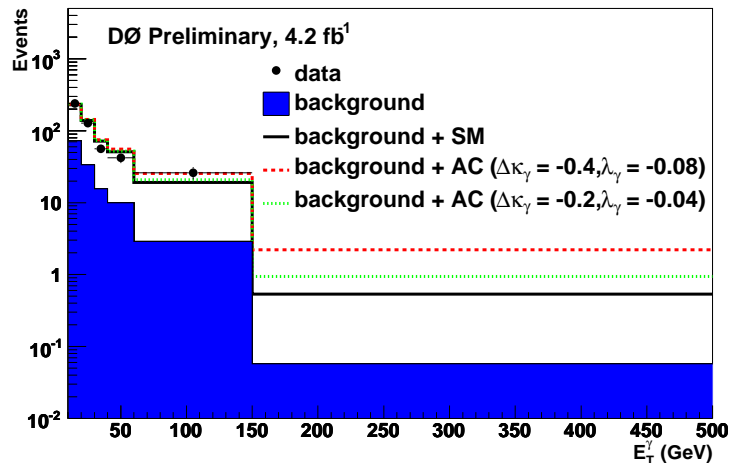


FIG. 5: Photon E_T spectrum for data, background, and SM signal, as well as two different AC MC events.

We also measure the cross section times branching fraction for the process $p\bar{p} \rightarrow W\gamma + X \rightarrow \mu\nu\gamma + X$ with $p_T^\gamma > 8$ GeV and $\Delta R_{\mu\gamma} > 0.7$. The SM prediction gives 16.0 ± 0.4 pb [2, 3] using CTEQ6L1 PDF. For this analysis, the cross section is obtained from the number of data events corrected for the background contribution, divided by the trigger, photon and muon selection efficiencies, acceptance, integrated luminosity. The cross section is measured to be $\sigma = 15.2 \pm 0.4$ (stat) ± 1.6 (syst) pb, which is in good agreement with the SM prediction.

VII. SUMMARY

The cross section times branching fraction for the process $p\bar{p} \rightarrow W\gamma + X \rightarrow \mu\nu\gamma + X$ with $p_T^\gamma > 8$ GeV and $\Delta R_{\mu\gamma} > 0.7$ is measured to be 15.2 ± 0.4 (stat) ± 1.6 (syst) pb, which agrees with the SM expectation of 16.0 ± 0.4 pb. We set limits on anomalous WW γ couplings using photon transverse energy distribution at the 95% C.L. The one dimensional 95% C.L. limits are $-0.14 < \Delta\kappa_\gamma < 0.15$ and $-0.02 < \lambda_\gamma < 0.02$. These are the most stringent limits at a hadron collider of this final state. We reach the similar sensitivity as the LEP experiments.

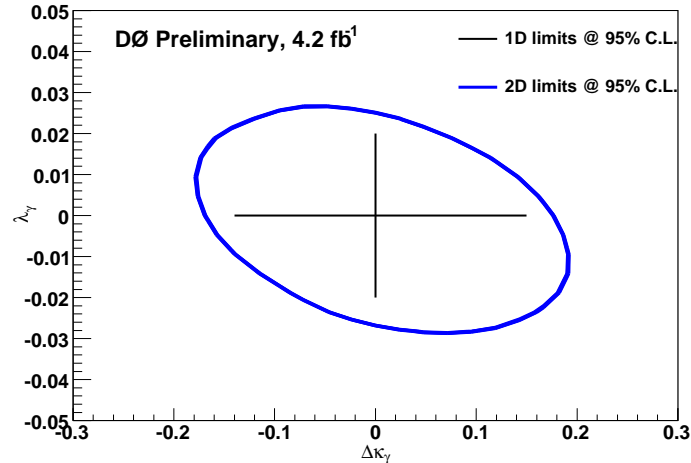


FIG. 6: 95% C.L. limits on $\Delta\kappa_\gamma$ and λ_γ . One dimensional 95% limits are represented by the horizontal and vertical lines.

Acknowledgments

We thank the staffs at Fermilab and collaborating institutions, and acknowledge support from the DOE and NSF (USA); CEA and CNRS/IN2P3 (France); FASI, Rosatom and RFBR (Russia); CAPES, CNPq, FAPERJ, FAPESP and FUNDUNESP (Brazil); DAE and DST (India); Colciencias (Colombia); CONACyT (Mexico); KRF and KOSEF (Korea); CONICET and UBACyT (Argentina); FOM (The Netherlands); STFC (United Kingdom); MSMT and GACR (Czech Republic); CRC Program, CFI, NSERC and WestGrid Project (Canada); BMBF and DFG (Germany); SFI (Ireland); The Swedish Research Council (Sweden); CAS and CNSF (China); and the Alexander von Humboldt Foundation.

-
- [1] T. Sjöstrand *et al.*, JHEP **0605**, 026 (2006).
 - [2] U. Baur, T. Han, J. Ohnemus, Phys. Rev. D **48**, 5140 (1993).
 - [3] U. Baur, S. Errede, G. Landsberg, Phys. Rev. D **50**, 1917 (1994).
 - [4] V. M. Abazov *et al.*, Nucl. Instrum. Meth. A **565**, 463 (2006).
 - [5] V. M. Abazov *et al.* (DØ collaboration), Phys. Rev. Lett. **102**, 231801 (2009).
 - [6] V. M. Abazov *et al.* (DØ collaboration), Phys. Lett. B **690**, 108 (2010).
 - [7] T. Andeen *et al.*, FERMILAB-TM-2365 (2007).
 - [8] J. Pumplin *et al.*, JHEP **0207**, 012 (2002).
 - [9] V. M. Abazov *et al.* (DØ collaboration), Phys. Rev. Lett. **100**, 241805 (2008).
 - [10] ALEPH Collaboration, Phys. Lett. B **614** (2005) 7;
 L3 Collaboration, Phys. Lett. B **586** (2004) 151;
 OPAL Collaboration, Eur. Phys. J.C. 33 (2004) 463;
 The LEP-TGC combination group, LEPEWWG/TGC/2004-01, January 2004.
<http://lepewwg.web.cern.ch/LEPEWWG/lepww/tgc/>